

COMPARATIVE STUDY OF SYSTEM IDENTIFICATION METHODS APPLIED TO AEROELASTIC MODELS TESTED IN WIND TUNNEL

Thiago H. L. Pinto, MSc^{*} , Roberto G. A. da Silva, Dr^{} , Guilherme R. Beghini, PhD^{***}**

^{*}UFVJM, Diamantina, Minas Gerais, Brazil,

^{}ITA, São José dos Campos, São Paulo, Brazil,**

^{*}Embraer, São José dos Campos, São Paulo, Brazil**

Keywords: *System Identification, Aeroelasticity, Structural Dynamics*

This work was funded by FAPEMIG and PROAPP-UFVJM.

Abstract

The use of tests is required when moving into areas sparsely explored by theory as an important tool for its validation. Aeroelastic wind tunnel tests using scaled models can be performed in order to verify the analytical methods, requiring a model that represents the problem qualitatively or, in a more complex case, checking the behavior of a real aircraft, requiring a representative model in which tests must necessarily be done demonstrating, statically and dynamically, their fidelity to the real structure. In this work, using previously acquired wind tunnel tests experimental data, a modal identification routine has been developed to analyse the data. Using theoretical scaled aircraft models, a theoretical versus experiment correlation was performed in order to verify the quality of the theoretical results.

1 Aeroelastic Model

Usually, an aeroelastic model is composed of aerodynamic and dynamic models, which are constructed separately. Interpolation of information between these models is made using splines. A sketch of the aeroelastic model representation is shown in Figure 1. In this work, the software Nastran [9] is used to represent the dynamic model (stiffness and mass distribution) and the

software ZAERO [11] is used to represent the aerodynamic model and the splines. The aerodynamic model of ZAERO employed in this work is the Zona6 method, which is based on the standard version of the Doublet Lattice Method implemented in Nastran. Both methods are discrete element methods, based on elementary solutions of the linearized aerodynamic potential equation [10]. The models are developed through the subdivision of the aerodynamic geometry in elements (also called panels), where the elementary solution associated with each of these elements equation is known. From composition of these elements and assuming the principle of superposition of potential effects one can obtain one solution to an aerodynamic load on the body.

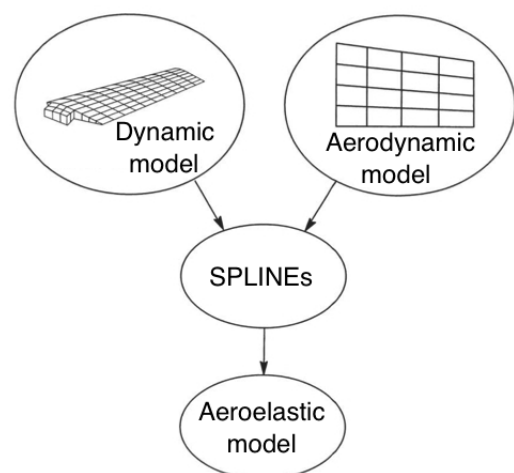


Fig. 1 : Aeroelastic model

Each panel is constructed such that both side edges are parallel to the unperturbed flow. A doublet polynomial acceleration distribution line of unknown intensity is positioned at 1/4 of the chord at each panel. The boundary condition is applied to 1/2 of the average chord of each panel (NASTRAN’s boundary condition is applied to 3/4). The method is used to numerically evaluate the aerodynamic influence coefficient matrix by determining the intensity of acceleration unknowns.

Once the aircraft finite element model typically contains a large number of degrees of freedom, the size of the mass and rigidity arrays is generally very large and thus it’s solution would be computationally very expensive. One way to reduce the problem’s computational cost is the introduction of the modal approach.

The rationale of the modal approach is based on the premise that critical vibration modes are generally due to the coupling of the structural modes of lower order. These modes usually have lower natural frequencies, thus requiring less energy in promoting the coupling between modes due unsteady aerodynamic load.

The conventional practice of flutter analysis is to formulate the aeroelastic system into a set of linear systems and determine their stability borders by solving the complex eigenvalues problem thus generated. This procedure involves the assumption of magnitude linearization of the structural displacement that considers that the aerodynamic response varies linearly with structural deformation amplitude of a given vibration mode of the aircraft, if the amplitude is sufficiently small.

With the results obtained by a Ground Vibration Test (GVT) made in the wind tunnel model, adjustments on the theoretical dynamic model can be taken. The Table 1 gives a brief description of each mode, the frequency values obtained for the GVT and the theoretical model, and the percentage error having as reference the GVT data.

In the Figure 2, we can observe graphically the correlation between the theoretical and GVT data. On this, for each mode, a point is plotted having as abscissa the frequency value obtained in GVT and, as ordinate, it’s theoretical

Table 1: Modal Description

Vibration Mode		GVT (Hz)	Model (Hz)	Delta %
Wing Bending 2N	SYM	28.72	29.27 (7)	1.93%
Wing Bending 1N	ASY	37.69	37.66 (8)	-0.07%
Engine Lateral	SYM	46.95	47.00 (9)	0.10%
Engine Lateral	ASY	48.52	48.47 (10)	-0.11%
Fuselage Lateral	ASY	55.9	53.27 (11)	-4.70%
Fuselage Vertical	SYM	59.5	57.26 (12)	-3.76%
Engine Vertical	SYM	64.95	64.84 (13)	-0.17%
Engine Vertical	ASY	66.76	66.92 (14)	0.24%
Fuselage Lateral 2	ASY	75.13	76.51 (15)	1.84%
Engine Roll	SYM	80.28	80.78 (16)	0.62%
Engine Roll	ASY	81.41	81.78 (17)	0.45%
Fuselage Torsion	ASY	89.72	88.43 (18)	-1.44%
Wing Bending 4N	SYM	97.09	90.19 (19)	-7.11%
Wing In Plane Bending	SYM	92.42	94.91 (20)	2.69%
Hstab/Vfin Bending	ASY	-	99.29 (21)	-
Hstab Bending	SYM	-	110.47 (22)	-

frequency. The dotted blue line is used as a reference for accurate correlation. The dashed black lines are used to mark the maximum acceptable error ($\pm 10\%$).

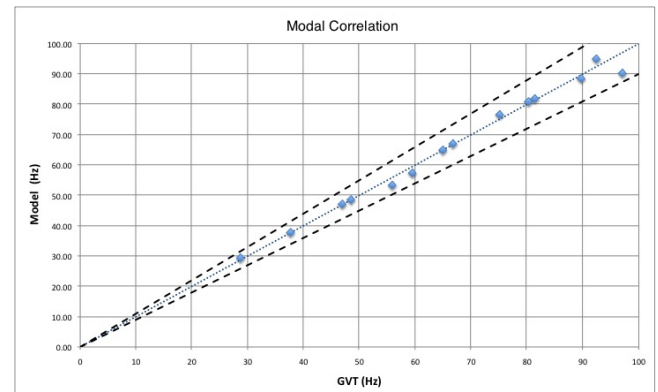


Fig. 2 : Modal Correlation

During the aeroelastic wind tunnel tests, five different engine pylons stiffness and wing tip mass balancing configurations were tested:

- vertical pylons stiffness 125% (P125) and lateral 100% (Y100), 50 kg of ballancing mass (M50kg) (reference);
- vertical pylons stiffness 125% (P125) and lateral 100% (Y100), 20 kg of ballancing mass (M20kg);
- vertical pylons stiffness 100% (P100) and lateral 100% (Y100), 50 kg of ballancing mass (M50kg);

Comparative study of system identification methods applied to aeroelastic models tested in wind tunnel

- vertical pylons stiffness 75% (P075) and lateral 100% (Y100), 50 kg of ballancing mass (M50kg);
- vertical pylons stiffness 100% (P100) and lateral 75% (Y075), 50 kg of ballancing mass (M50kg).

The figures 3a and 3b presents the results of these configurations for the main aeroelastic asymmetrical modes, at Mach 0.8 and Mach 0.9, respectively. Following, figures 3c and 3d presents the results of these configurations for the main aeroelastic symmetrical modes, at Mach 0.8 and Mach 0.9, respectively.

2 System identification method

The identification process implemented in this work in order to perform the identification of aeroelastic systems tested in the wind tunnel can be described, in a simplified way, by the block diagram shown in Figure 4.

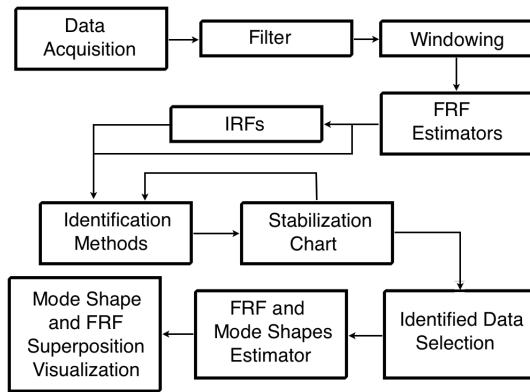


Fig. 4 : Identification process block diagram

The starting routine is responsible for data acquisition, reading and interpreting of the input data files. At this stage it is also chosen the sensors and ranges to be used in the system identification to be performed, and the wind tunnel anemometer data verification is performed.

During the signals analysis, aliasing, Bias and Leakage effects, along with wind tunnel test noise, may cause identification results outside the frequency range employed as input. In order to

minimize this effect a band-pass filter was implemented, in which the range of excitation was chosen as the minimum and maximum cutoff frequency.

A bandpass filter can be built from the convolution between a low-pass filter and a high-pass filter, and may, in the frequency domain, be defined as Equation 1 [3]:

$$G_x(f) = a; \quad f_{min} \leq f \leq f_{max} \\ = 0; \quad f < f_{min} \text{ ou } f > f_{max} \quad (1)$$

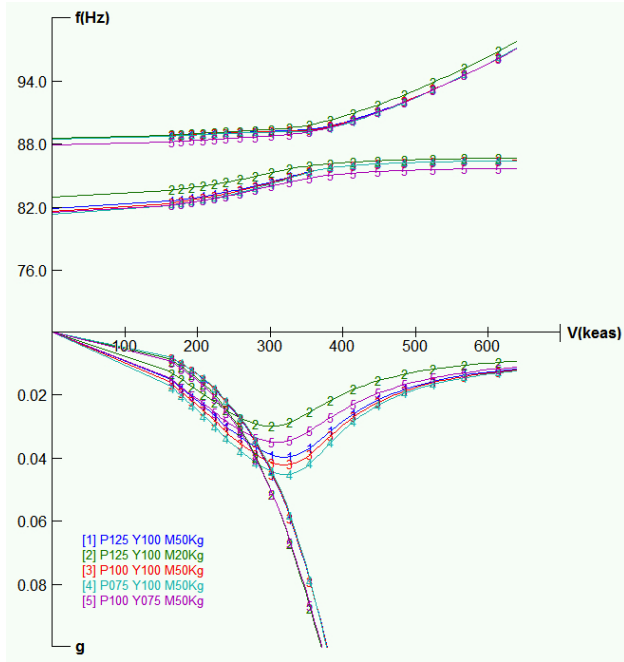
Using windowing techniques, one can set the length of the observation of a sampled signal. If we consider a random noise signal, and knowing that the average of a random signal tends to zero, we can conclude that the windowing can reduce the noise effects by enabling the achievement of means between the parts of the signal (windows). Windowing techniques can also be performed in order to minimize effects such as Leakage [6]. For this purpose the window function employed should be chosen such that the ends of each cutout signal tend to zero, thereby minimizing the effect of the signal truncation.

Apply a window to a signal in the time domain is equivalent to multiplying the signal by the function that represents the window. Owing to the fact that multiplication in the time domain is equivalent to convolution in the frequency domain, the spectrum of a windowed signal is the convolution of the original signal spectrum with the spectrum of the window. Thus, the windowing modifies the signal shape in both time domain and in frequency [1].

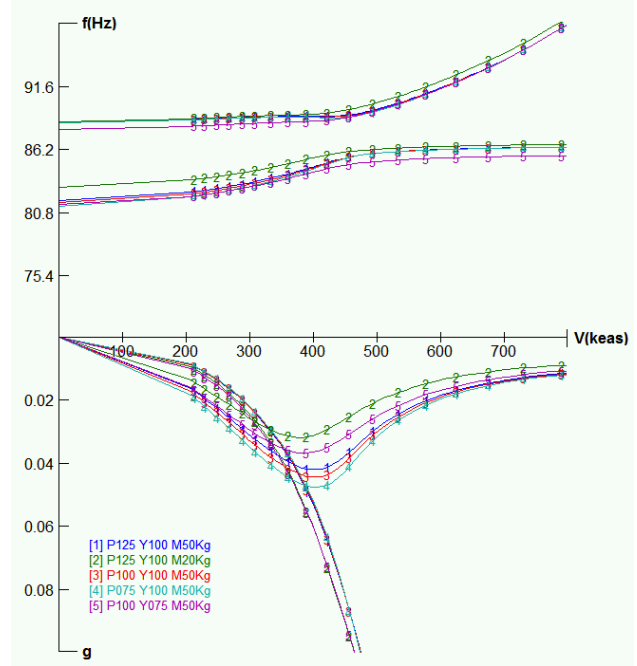
The Hanning window used in this work, a general purpose window commonly recommended for continuous signals, mathematically can be set by Equation 2 [8]:

$$W_f(t) = \frac{1}{2} \left[1 + \cos \left(\frac{2\pi t}{T} \right) \right]; \quad |t| \leq \frac{T}{2} \\ = 0; \quad |t| > \frac{T}{2} \quad (2)$$

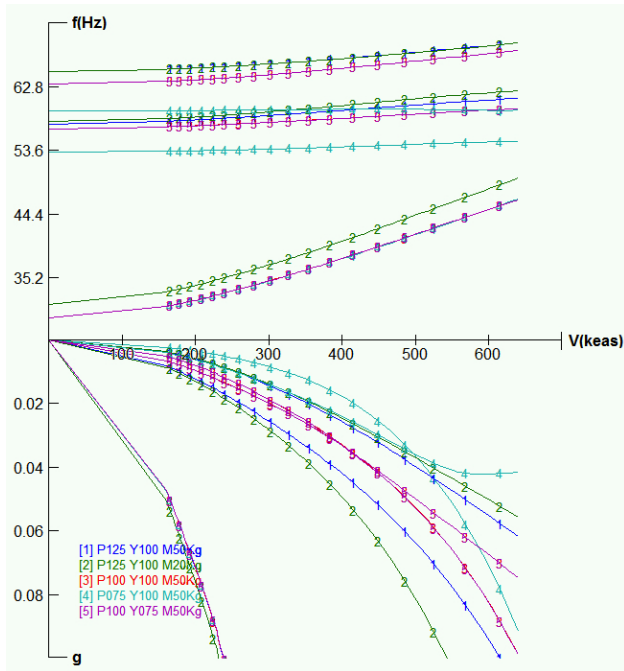
In order to compensate the distortion produced by the windowing, it is necessary to multiply the windowed FFT signal by a correction



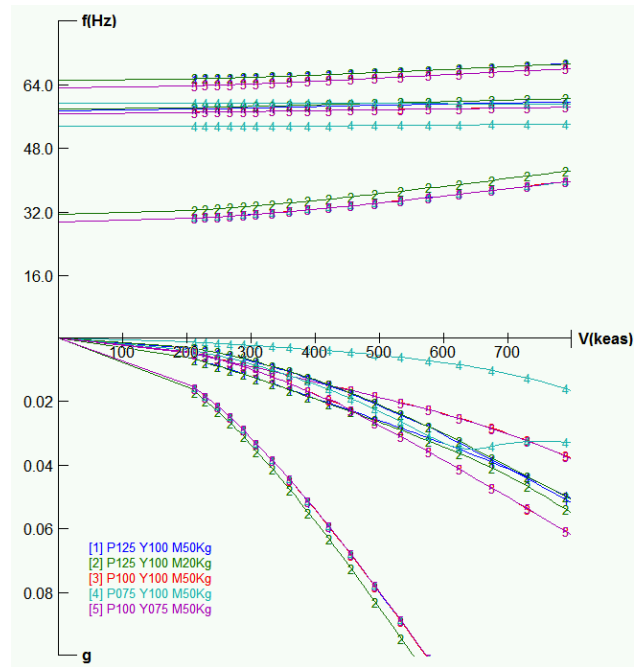
(a) VGF Mach 0.80 ASY



(b) VGF Mach 0.90 ASY



(c) VGF Mach 0.80 SYM



(d) VGF Mach 0.90 SYM

Fig. 3 : Studied cases theoretical aeroelastic results

factor. For the Hanning window, the correction factor is given by Equation 3.

$$F_{cor} = 2\sqrt{\frac{8}{3}} \quad (3)$$

This factor is composed by the multiplication between correction factors responsible for the amplitude degradation (2) and energy degradation ($\sqrt{\frac{8}{3}}$).

The Frequency Response Function, or FRF of

a system can be seen as a filter function, created by the system and applied to the excitation input [2]. This contains the information for each of the vibration modes and resonance frequencies related. In possession of the system's FRFs, it's possible to achieve it's impulse response functions (IRFs), which can be defined as the response of the dynamical system, in the time domain, to an impulsive input signal [8].

Four system identification methods were implemented in the system identification routine developed in this work. Three of them in time domain: Least Squares Complex Exponential (LSCE [8]), Eigensystem Realisation Algorithm (ERA [8]) and Eigensystem Realisation Algorithm with Data Correlation (ERA-DC [5]); and one in frequency domain: Rational Fraction Polynomial (RFP [8]).

Then it's necessary to select the results to proceed with the routine. A stabilization chart is a tool often used to assist in the splitting between real and mathematical poles [7]. The mathematical poles are generated due to the fact that identification methods generally employ the concept of oversizing for dealing with noise, so that the estimations are obtained for a larger number of modes than that actually present on system response. Through the stabilization diagram, by the user interface, the visually stable data selection is performed.

In possession of the identified data by the above methods, the Least Squares Frequency Domain method (LSFD, [4]) was used to estimate the identified FRFs and mode shapes of the tested model.

The signal used as excitation for this system is composed of a sequency of sinusoidal 2 seconds pulses, ranging from 20Hz to 100Hz approximately. It can be seen in the Figure 5 this signal along time and, in the bottom part of this figure, it's PSD (Power Spectral Density).

The signal is then supplied to two moving masses inserted into the fuselage, providing both symmetrical and asymmetrical physical excitation to the model. The figures 6a and 6c shows, for the symmetric and asymmetric excitation cases, respectively, a 5 seconds time domain cut relative to the input signal, for both left and

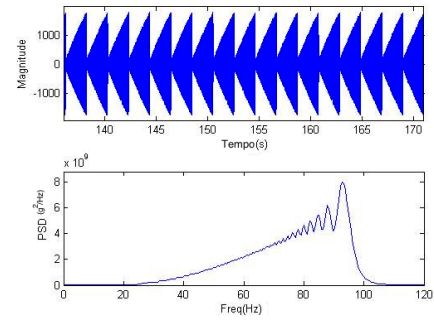


Fig. 5 : Input signal.

right excitation masses. Then, in figures 6b and 6d, one can observe the amplitude, phase and coherence of the generated FRFs between the left and right excitation signal, and also the PSD of both input signals.

Since either emerge from the same excitations signal, it can be observed that the coherence between the signals tends to 1 over the entire range of excitation. This fact implies that these are not linearly independent excitations, then not being valid for multiple input methods (MIMO), leading, for this work, the choice between SISO and SIMO methods. The use of multiple excitations, however, is a device for inject a higher amount of energy in the system, leading to an easier test execution.

In either the symmetrical and asymmetrical excitation cases, one can observe that the range varies from 20Hz to 100Hz. Since these values are kept throughout all the tested cases, it was implemented a band pass filter, using them as lower and upper limits, in order to minimize noise in the results.

In order to show the windowing effect over the signal conversion from time to frequency domain, FRF's magnitude and phase, coherence and PSD of input and output signals are presented. The left excitation channel was used as input and the right wing bending channel was used as output. 7a presents these data without any treatment, where one can observe the high noise level.

In these tests, the data acquisition was performed at a 500Hz rate, thus being 250Hz the Nyquist cutoff frequency used as the maximum

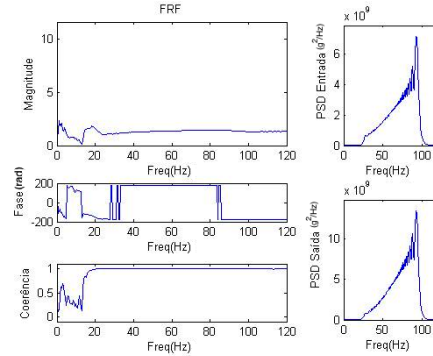
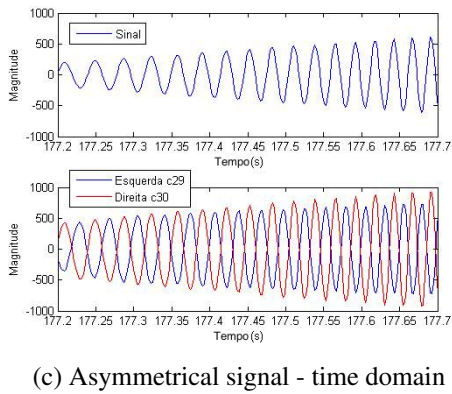
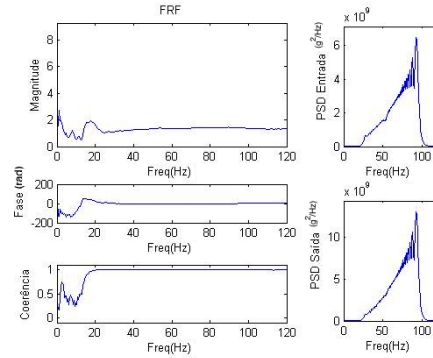
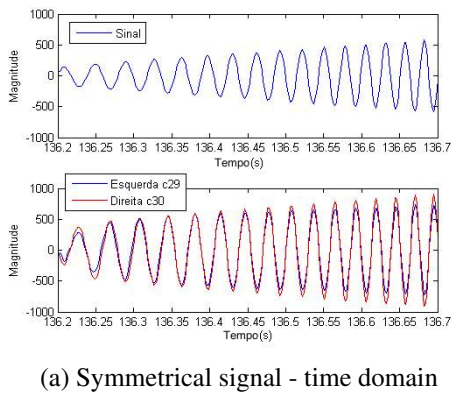


Fig. 6 : Input digital signal

frequency of the presented FRFs.

In order to minimize the noise effect within the excitation range, windowing was applied in order to enable the use of averages in input and output signals since, considering the noise a random input, it's average tends to zero, generating responses with higher level of coherence in relation to the inputs. The figure 7b presents the above data, where a 1024 points rectangular windowing (simple cutouts of the signals) was used as window, with no overlap between windows.

One bandpass filter, accomplished by Fourier transform, was used over input and output data, in order to eliminate noise peaks in the FRF out of input excitation range. The figure 7c shows the same data as the previous example, where this bandpass filter was turned on. It can be seen that there are virtually no out of excitation band results, and inside of this range, the coherence is quite high, indicating that the modes excitation are actually occurring in response to the input.

Rearranging the frequency scale to 20 Hz to 100 Hz, we have the figure 7d.

The figure 7e can be generated using the same rectangular window, with 80% of overlap between windows. It is observed that for this type of window, the effect of the number of overlapping windows is fairly noticed being only an increase in the number of performed averages.

In order to verify separately the influence of windowing and overlapping, the figure 7f presents the same data using a 1024 points Hanning window without overlapping. Observing the signals' PSDs, there is a input signal degradation due to the windowing use, without the use of means, in a system with a pulse input signal near coinciding the number of points per pulse (2 seconds pulses with a 500 Hz sample) with the window size (1024 dots). This causes the degradation effect seen in the input signal PSD, since the beginning and the end of each pulse is in the same low factor Hanning region.

Comparative study of system identification methods applied to aeroelastic models tested in wind tunnel

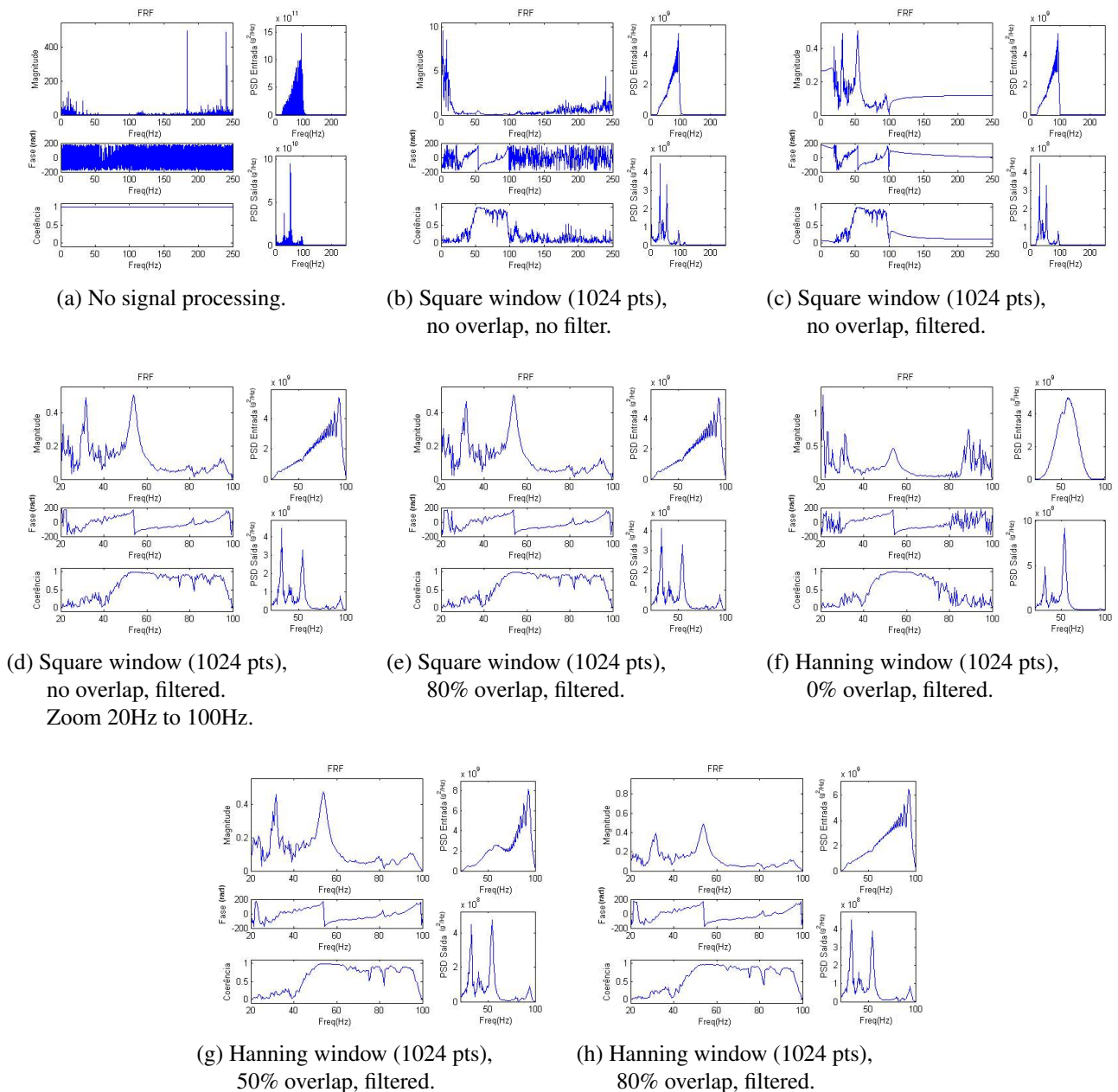


Fig. 7 : Signal processing example.

The figure 7g has the same check using a 1024 points Hanning window with 50% of overlap. When inserting overlap between windows, so that the start pulse not always coincide near the beginning of a window, it is observed that the degradation effect is fairly low.

Finally, the figure 7h have the same verification using a 1024 points Hanning window with 80% of overlap. With the percentual overlap, which leads to an increase in the number

of means and variability in relative positions between windows and pulses, one can observe that the aforementioned effect nearly disappears.

Comparing the results using a Hanning window with 80% overlap (figure 7h), with those obtained using the rectangular window with the same overlap (figure 7e), one can observed that noise is considerably lower with the Hanning window use. This noise reduction is due to the fact that, with the Hanning window use, well be-

haved cutouts signal were obtained by forcing it's ends to values near zero, thus minimizing the leakage effect due to incomplete periods.

From the filtered and windowed signal presented in figure 7h, it is possible to continue the identification routine. The risk to come across this problem could be reduced if the test were performed with the use of a random or burst signal excitation, thus increasing the input randomness.

3 Comparison of Theoretical versus Experimental Results

The following charts shown the superposed results for theoretical and experimental models. In order to obtain a direct comparison between the model and wind tunnel data, the values of the dynamic pressure, rather than calibrated airspeed, were used in the abscissa axis below.

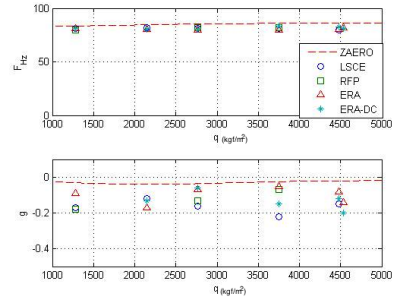
Considering the reference configuration (P125 Y100 M50Kg), identifications for Mach 0.8 were performed for the modes that compose the main symmetric and asymmetric aeroelastic mechanisms described by theoretical analysis.

The asymmetric mechanism is presented by Figure 8. Figures 8a and 8b shown identified modal evolution for the asymmetric engine roll and asymmetric fuselage torsion, respectively, both for Mach 0.8.

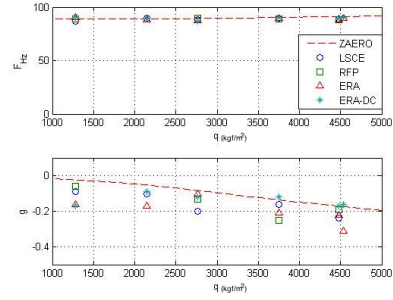
Following, the symmetric mechanism is presented by Figure 9. Figures 9a, 9b and 9c shown identified modal evolution for the symmetric wing bending 2N, fuselage vertical bending and symmetric engine vertical bending, respectively, for Mach 0.8.

It can be observed from the identified VGF curves a low identified frequency dispersion and a low level of theoretical error in relation to identified data.

One can observe a reasonable damping data dispersion and a tendency to obtain lower theoretical absolute values. The experimental values dispersion is due the great influence that the sources of error have on them, since the damping factors are defined by the shape presented by the FRFs and IRFs. The lower absolute damping levels tendency in the theoretical model is due to the



(a) Engine Roll Asy.



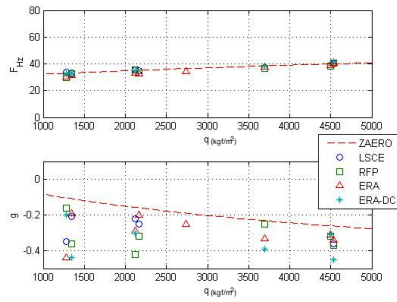
(b) Fuselage Torsion Asy.

Fig. 8 : Theoretical and experimental results for main asymmetrical modes (Mach 0.80; P125 Y100 M50).

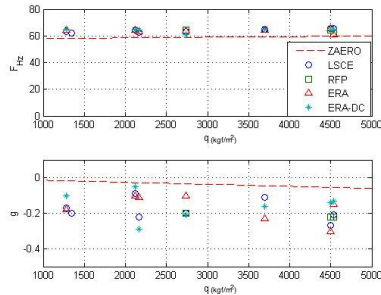
conservative assumption of neglecting the structural damping in the theoretical modeling.

An attempt to evaluate the performance of the identification methods was made by computing the success or failure of each method, as shown in Table 2. Each row in this table represents one VGF theoretical versus experimental aeroelastic model correlation. The cases column refers to the number of dynamic pressure points chosen for the identifications. In the following columns are displayed, for each identification method, the number of performed successful identifications, and it's respective percentage of success. The final line of this table presents the total cases and successes, and their percentages, for each system identification method.

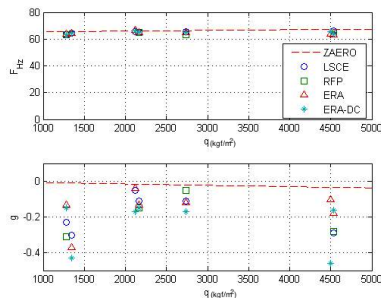
Comparative study of system identification methods applied to aeroelastic models tested in wind tunnel



(a) Wing Bending 2N Sym.



(b) Fuselage Vertical Bending.



(c) Engine Vertical Sym.

Fig. 9 : Theoretical and experimental results for main asymmetrical modes (Mach 0.80; P125 Y100 M50).

Due to the low number of samples and the human factor influence, one can not directly conclude whether one method is better or worse than another. However, in the studied cases, there was a greater difficulty in performing stabilized identifications with the RFP method, which is also the one with highest computational cost. In turn, the ERA method, and his ERA-DC extension presented in these analyzes, have presented higher success rates, without a computational cost as high as the RFP. At last LSCE method, with it's simple implementation, have presented a reason-

able success rate and a low computational cost, being a good option if all these factors are taken into account.

4 Conclusions

In this work one can observed the importance of signal processing in performing aeroelastic wind tunnel tests analysis in order to minimize the analysis' noise effects and errors.

Based on the correlation between theoretical and experimental results, one can observe a low dispersion between the identified frequency data, and that the theoretical data show a relatively low level of error in relation to those data. It's still possible to observe a reasonable damping dispersion, due to the great influence exercised by the sources of error, and a tendency to achieve lower levels of damping in the theoretical model due to the conservative assumption, adopted during theoretical modeling, of neglecting the structural damping.

In comparing system identification methods, issues such as the percentage of successful identification cases, computational cost and complexity of the method were observed, however, due to the low number of samples and the human factor influence, such analyzes are shown inconclusive when attempting to elect one as the most efficient method.

Acknowledgments

The first and second authors acknowledge the partial support from the Instituto Nacional de Ciência e Tecnologia - Estruturas Inteligentes em Engenharia, INCT-EIE, the Conselho Nacional de Desenvolvimento Científico e Tecnológico, CNPq, and also the Fundação de Amparo à Pesquisa do Estado de Minas Gerais, FAPEMIG, from Brazil.

The first and third authors acknowledge the partial support from Embraer.

Table 2: Rate of successful identification for each method.

Configs.	MACH	Mode		Test cases	Cases with successful identification							
					LSCE		RFP		ERA		ERA-DC	
p125y100m50	80	7	SYM	8	5	63%	7	88%	8	100%	6	75%
		12	SYM	8	8	100%	3	38%	7	88%	7	88%
		13	SYM	8	6	75%	4	50%	7	88%	7	88%
		17	ASY	6	5	83%	3	50%	6	100%	6	100%
	18	ASY	6	5	83%	4	67%	6	100%	6	100%	
	90	17	ASY	5	5	100%	4	80%	5	100%	5	100%
P125Y100m20	80	17	ASY	5	5	100%	4	80%	5	100%	5	100%
	90	17	ASY	5	4	80%	3	60%	5	100%	3	60%
P100Y100m50	80	17	ASY	5	5	100%	4	80%	5	100%	5	100%
	90	17	ASY	5	4	80%	4	80%	4	80%	5	100%
P075Y10050	80	17	ASY	5	5	100%	4	80%	4	80%	4	80%
	90	17	ASY	5	4	80%	5	100%	4	80%	5	100%
P100Y0755	80	17	ASY	5	3	60%	3	60%	4	80%	3	60%
	90	17	ASY	5	5	100%	4	80%	4	80%	5	100%
Total				81	69	85%	56	69%	74	91%	72	89%

References

- [1] Andrade A O, Soares A B, Técnicas de Janelamento de Sinais. In: *Seminário do estudantes de engenharia elétrica da UFU*, 3., 2000, Uberlândia, Anais..., 2000, pp. 16?18, Uberlândia: UFU.
- [2] Avitabile P, MODAL SPACE - IN OUR OWN LITTLE WORLD: What is a good MAC value so I know my model is right? In: *SEM Experimental Techniques*, 2006, pp. 2.
- [3] Bendat J, Piersol A, *Random Data*, Wiley-Interscience, analysis and measurement procedures. New York, 1971.
- [4] Benini G R, *Detection and Identification of Nonlinearities for Flight Flutter Testing*, Ph.D. thesis, School of Mechanical, Aerospace , Civil Engineering, University of Manchester, Manchester, 2006.
- [5] Cooper J E, Wright J R, Spacecraft in-orbit identification using eigensystem realisation methods, *Journal of Guidance, Control and Dynamics*, Vol.15, No.2, pp. 352-359, 1992.
- [6] Ewins D J, *Modal Testing*, Research Studies Press LTD., theory and practice. London, 1984.
- [7] Guillaume P, *Modal Analysis*, Master's thesis, Vrije Universiteit Brussel, Belgium, 2005.
- [8] Maia N M M, Silva J M M, *Theoretical and Experimental Modal Analysis*, Research Studies Press, London, 1997.
- [9] MSC NASTRAN *Version 68 - Aeroelastic Analysis User's Guide*. MSC SOFTWARE CORPORATION, 2002.
- [10] Silva R G A, *A study on correction methods for aeroelastic analysis in transonic flow*, Ph.D. thesis, Departamento de Aerodinâmica, Propulsão e Energia, Instituto Tecnológico de Aeronáutica, São José dos Campos, 2004.
- [11] ZAERO *Version 8.5 - Theoretical manual*, Scottsdale: Zona Technology Inc., 2011.

Contact Author Email Address

To contact the author, send an email to the address: thiago.lara@ict.ufvjm.edu.br.

Copyright Statement

The authors confirm that they, and/or their company or organization, hold copyright on all of the original material included in this paper. The authors also confirm that they have obtained permission, from the copyright holder of any third party material included in this paper, to publish it as part of their paper. The authors confirm that they give permission, or have obtained permission from the copyright holder of this paper, for the publication and distribution of this paper as part of the ICAS 2014 proceedings or as individual off-prints from the proceedings.